J. Cent. South Univ. (2016) 23: 484−496
DOI: 10.1007/s11771-016-3094-0

Springer

Heat transfer of copper/water nanofluid flow through converging-diverging channel

Mohamed Rafik SARI[1, 2], Mohamed KEZZAR[1], Rachid ADJABI[2]

1. Mechanical Engineering Department, University of Skikda, El Hadaiek Road, B. O. 26, 21000 Skikda, Algeria;
2. Industrial Mechanics Laboratory, Badji-Mokhtar University of Annaba, B. O. 12, 23000 Sidi Amar Annaba, Algeria

Abstract: The main objective of this work is to investigate analytically the steady nanofluid flow and heat transfer characteristics between nonparallel plane walls. Using appropriate transformations for the velocity and temperature, the basic nonlinear partial differential equations are reduced to the ordinary differential equations. Then, these equations have been solved analytically and numerically for some values of the governing parameters, Reynolds number, *Re*, channel half angle, α, Prandtl number, *Pr*, and Eckert number, *Ec*, using Adomian decomposition method and the Runge-Kutta method with mathematic package. Analytical and numerical results are searched for the skin friction coefficient, Nusselt number and the velocity and temperature profiles. It is found on one hand that the Nusselt number increases as Eckert number or channel half-angle increases, but it decreases as Reynolds number increases. On the other hand, it is also found that the presence of Cu nanoparticles in a water base fluid enhances heat transfer between nonparallel plane walls and in consequence the Nusselt number increases with the increase of nanoparticles volume fraction. Finally, an excellent agreement between analytical results and those obtained by numerical Runge-Kutta method is highly noticed.

Key words: nanofluid flow; heat transfer; copper nanoparticles; inclined walls; analytical solution

1 Introduction

The steady two-dimensional flow of an incompressible, viscous fluid between nonparallel plane walls separated by an angle 2α driven by a line source or sink provides one of the few exact solutions of the Navier-Stokes equations. The nonlinear governing equation of this flow was given by JEFFERY [1] and independently by HAMEL [2]. Thereafter, several contributions were undertaken by many researchers in order to solve the nonlinear problem of Jeffery-Hamel flow. The study done by ROSENHEAD [3] gives the solution in terms of Jacobian elliptic functions. The exact solution of the energy equation governing thermal distributions between nonparallel plane walls was explored by MILLSAPS and POHLHAUSEN [4]. They calculated temperature profiles only due to dissipation. FRAENKEL [5] studied laminar flow in symmetrical channels with slightly curved walls. This study gives the solution of the velocity profile as a power series. SHEIKHOLESLAMI et al [6] studied the effects of magnetic field and nanoparticles on the Jeffery-Hamel flow using Adomian decomposition method. Their results show an excellent agreement with those of numerical Runge-Kutta method. HATAMI et al [7] used different analytical methods for solving the equation governing the magneto-hydrodynamic (MHD) Jeffery-Hamel nanofluid flow. They found that the last square method (LSM) is more accurate in obtaining the solution of the studied problem. The research done by ELLAHI et al [8] gives a theoretical study dealing with the effects of magnetohydrodynamic on the peristaltic flow of Jeffery fluid in a rectangular duct through a porous medium. They solved analytically the governing equations of the studied problem, and, demonstrated that their results are in excellent agreement with those reported in literature. According to Refs. [9–11], many researchers also discussed the nonlinear problem of Jeffery-Hamel flow.

Nowadays, it is well established that the nanofluids are considered as a highly efficient class of heat transfer fluids. This novel category of fluids is generated by dispersing ultrafine particles (less than 100 nm) like Cu, CuO, Al_2O_3 and SiC in a conventional base fluid such as water, ethylene glycol and engine oil. The first use of nanofluid term is given by CHOI [12]. Since then, there has been an increasing interest in the analysis of nanofluids. We can easily find a wide number of experimental and theoretical studies dealing with

Received date: 2015−03−10; **Accepted date:** 2015−06−15
Corresponding author: Mohamed Rafik SARI; Tel: 00213661778242; E-mail: sari_rafik10@yahoo.fr

nanofluids. Experimentally, a particular attention was dedicated to the measurement of thermal conductivity for different nanofluids [13–16]. In fact, researchers found that the nanofluids exhibit significantly higher thermal conductivities than base fluids. On the other hand, nanofluids were widely used as heat transfer fluids in many configurations, especially in heat exchangers. With this intent, PAK and CHO [17] studied turbulent friction and heat transfer characteristics of several nanofluids in a circular pipe. XUAN and LI [18] undertook an experimental study on an original test rig. They investigated flow performance and convective heat transfer of Cu-water nanofluid for turbulent flow in a circular pipe. HE et al [19] also studied experimentally nanofluid flow and heat transfer characteristics through a straight vertical pipe for both laminar and turbulent flow. The convective heat transfer behaviour of nanofluid flow through horizontal tube heated by a constant heat flux was studied by TORII and YANG [20].

Theoretically, the effect of nanoparticles on heat transfer characteristics was studied. SHEIKHOLESLAMI and GANJI [21] investigated analytically, by homotopy perturbation method, heat transfer of Cu-water nanofluid flow between parallel plates. They found that their results are in excellent agreement when being compared with other numerical methods. KHANAFER et al [22] in their numerical investigation showed that nanoparticles enhanced significantly heat transfer rate at any given Grashof number. KUZNETSOV and NIELD [23] also studied natural convection of nanofluids flow past a vertical semi-infinite plate. SHEIKHOLESLAMI [24] used the KKL correlation for simulation of nanofluid flow and heat transfer in a permeable channel. The obtained results showed that the heat transfer enhancement is mainly related to the Reynolds number when power law index is equal to zero. Ferrofluid flow and heat transfer under the effect of spatially variable magnetic field were also investigated by SHEIKHOLESLAMI [25]. In fact, this study uses the control volume based finite element method (CVFEM) to investigate the effects of active parameters. The problem of nanofluid flow and heat transfer between parallel plates considering Brownian motion in the presence of variable magnetic field were studied analytically by SHEIKHOLESLAMI and GANJI [26] using differential transformation method. Their results showed on one hand that skin friction coefficient increases with an increase of squeeze number and Hartmann number, while it decreases as nanoparticle volume fraction increases. On the other hand, obtained results also demonstrated that Nusselt number is an increasing function of nanoparticle volume fraction and Hartmann number, but it is a decreasing function of the squeeze number. The magnetohydrodynamic free convection flow of CuO-water nanofluid in a square enclosure with a rectangular heated body was investigated numerically by SHEIKHOLESLAMI and GANJI [27] using lattice Boltzmann method. In fact, this investigation examines the effects of active parameters on the flow, heat transfer and the entropy generation, and, the results reveal that the heat transfer rate and the entropy generation number increase with increase of nanoparticle volume fraction and the Reynolds number; however, they are decreasing functions of Hartmann number. SHEIKHOLESLAMI and GANJI [28] also studied ferrofluid flow and heat transfer under the effect of an external magnetic field in a semi annulus enclosure with sinusoidal hot wall using control volume based finite element method (CVFEM). They investigated the effects of Rayleigh number, nanoparticle volume fraction, Magnetic number and Hartmann number on flow and heat transfer characteristics.

In recent years, several methods were developed in order to solve analytically the nonlinear initial or boundary value problem, such as the homotopy method [29–30], the variational iteration method [31–32] and the Adomian decomposition method [33]. These methods have been successfully applied for solving mathematical and physical problems [34–36]. On the other hand, many authors [37–40] have used these new approximate analytical techniques to investigate the nonlinear problem of Jeffery-Hamel flow.

In this work, the solution of steady two-dimensional flow of Cu-water nanofluid between nonparallel plane walls is presented. The resulting nonlinear ordinary differential equations governing velocity and heat transfer are solved analytically by an efficient technique of computation, called Adomian decomposition method and the obtained results are compared to the numerical Runge-Kutta solution. The principal aim of this work is to find approximate analytical solution of Jeffery-Hamel flow of Cu-water nanofluid in convergent and divergent channels.

2 Problem statement and governing equations

In this work, steady nanofluid flow and heat transfer between nonparallel plates are investigated analytically using the Adomian decomposition method. The geometry configuration of the Jeffery-Hamel flow of nanofluids is given in Fig. 1. In fact, the considered flow is uniform along z-direction and we assume purely radial motion, i.e., for velocity components we can write $V_r=V(r, \theta)$; $V_\theta=V_z=0$.

In vector form, the continuity equation, Navier-Stokes equation and energy equation for Jeffery-Hamel flow of nanofluids are expressed as

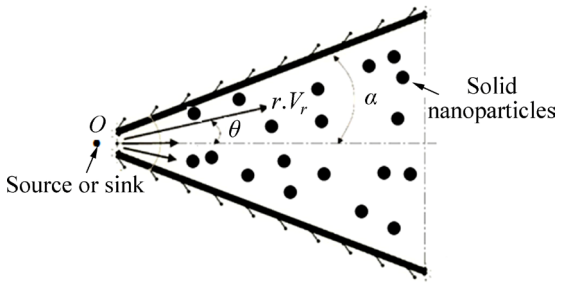

Fig. 1 Geometry of Jeffery-Hamel nanofluid flow

$$\nabla \boldsymbol{V} = 0 \tag{1}$$

$$\rho_{\mathrm{nf}} \cdot [(\boldsymbol{V}\nabla)\boldsymbol{V}] = -\nabla \boldsymbol{P} + v_{\mathrm{nf}} \cdot \Delta \boldsymbol{V} \tag{2}$$

$$(\rho \cdot c_p)_{\mathrm{nf}} \cdot (\boldsymbol{V}\nabla)\boldsymbol{T} = \phi + K_{\mathrm{nf}} + \nabla^2 \boldsymbol{T} \tag{3}$$

where $\boldsymbol{V}$ is the velocity vector, $\boldsymbol{T}$ is the temperature, ρ_{nf} is the effective nanofluid density, v_{nf} is the effective kinematic viscosity of nanofluid, $\boldsymbol{P}$ is fluid pressure, $(c_p)_{\mathrm{nf}}$ is the effective specific heat of nanofluid at constant pressure and K_{nf} is the effective nanofluid thermal conductivity.

The term ϕ on the right-hand side of Eq. (3) is the viscous dissipation term and is given by

$$\phi = \mu_{\mathrm{uf}}[2\varepsilon_{rr}^2 + 2\varepsilon_{\theta\theta}^2 + \varepsilon_{r\theta}^2] \tag{4}$$

The components of the strain tensor are given as

$$\begin{cases} \varepsilon_{rr} = \dfrac{\partial V_r}{\partial r} \\ \varepsilon_{\theta\theta} = \dfrac{1}{r} \cdot \dfrac{\partial V_\theta}{\partial \theta} + \dfrac{V_r}{r} \\ \varepsilon_{r\theta} = \dfrac{1}{r} \cdot \dfrac{\partial V_r}{\partial \theta} + \dfrac{\partial V_\theta}{\partial r} - \dfrac{V_\theta}{r} \end{cases} \tag{5}$$

In cylindrical coordinates (r, θ, z), the reduced forms of continuity, Navier-Stokes and energy equations are given by

$$\frac{\rho_{\mathrm{nf}}}{r} \cdot \frac{\partial}{\partial r}(rV_r) = 0 \tag{6}$$

$$V_r \cdot \frac{\partial V_r}{\partial r} = -\frac{1}{\rho_{\mathrm{nf}}} \cdot \frac{\partial p}{\partial r} + v_{\mathrm{nf}} \cdot \left[\frac{\partial^2 V_r}{\partial r^2} + \frac{1}{r} \cdot \frac{\partial V_r}{\partial r} + \frac{1}{r^2} \cdot \frac{\partial^2 V_r}{\partial \theta^2} - \frac{V_r}{r^2} \right] \tag{7}$$

$$-\frac{1}{\rho_{\mathrm{nf}} \cdot r} \cdot \frac{\partial p}{\partial \theta} + \frac{2v_{\mathrm{nf}}}{r^2} \cdot \frac{\partial V_r}{\partial \theta} = 0 \tag{8}$$

$$(\rho \cdot c_p)_{\mathrm{nf}} V_r \frac{\partial T}{\partial r} = K_{\mathrm{nf}} \left[\frac{1}{r} \frac{\partial}{\partial r}\left(r \frac{\partial T}{\partial r} \right) + \frac{1}{r^2} \frac{\partial^2 T}{\partial \theta^2} \right] + \mu_{\mathrm{nf}} \left[2\left(\left(\frac{\partial V_r}{\partial r} \right)^2 + \left(\frac{V_r}{r} \right)^2 \right) + \left(\frac{1}{r} \frac{\partial V_r}{\partial r} \right)^2 \right] \tag{9}$$

The effective density ρ_{nf}, the effective dynamic viscosity μ_{nf}, the effective heat capacity $(\rho \cdot c_p)_{\mathrm{nf}}$ and the effective thermal conductivity K_{nf} of the nanofluid are given as

$$\begin{cases} \rho_{\mathrm{nf}} = (1-\psi)\rho_{\mathrm{f}} + \psi\rho_{\mathrm{s}} \\ \mu_{\mathrm{nf}} = \dfrac{\mu_{\mathrm{f}}}{(1-\psi)^{2.5}} \\ (\rho \cdot c_p)_{\mathrm{nf}} = (1-\psi) \cdot (\rho \cdot c_p)_{\mathrm{f}} + \psi \cdot (\rho \cdot c_p)_{\mathrm{s}} \\ \dfrac{K_{\mathrm{nf}}}{K_{\mathrm{f}}} = \dfrac{(k_{\mathrm{s}} + 2k_{\mathrm{f}}) - 2\psi(k_{\mathrm{f}} - k_{\mathrm{s}})}{(k_{\mathrm{s}} + 2k_{\mathrm{f}}) + \psi(k_{\mathrm{f}} - k_{\mathrm{s}})} \end{cases} \tag{10}$$

where ψ is the volume fraction of nanoparticles, the subscript "f" denotes the base fluid and "s" the solid nanoparticles.

Now, introduce the following parameters:

$$F(\eta) = \frac{f(\theta)}{u_{\mathrm{c}}},\ \frac{T}{T_{\mathrm{W}}} = \frac{G(\theta)}{r^2},\ \eta = \theta/\alpha \tag{11}$$

where T_{W} is the constant wall temperature, and u_{c} is the rate of movement in the radial direction ($u_{\mathrm{c}} = r \cdot V_{\max}$).

And eliminating the pressure term between Eq. (7) and Eq. (8), we obtain

$$F''' + 2Re \cdot \alpha \cdot [(1-\psi)^{2.5} \cdot (1 - \psi + \psi \frac{\rho_{\mathrm{s}}}{\rho_f})] \cdot FF' + 4\alpha^2 F' = 0 \tag{12}$$

$$G'' + 4\alpha^2 G + \frac{(1-\psi) + \psi \dfrac{\rho_{\mathrm{s}} \cdot (c_p)_{\mathrm{s}}}{\rho_{\mathrm{f}} \cdot (c_p)_{\mathrm{f}}}}{\dfrac{(k_{\mathrm{s}} + 2k_{\mathrm{f}}) - 2\psi(k_{\mathrm{f}} - k_{\mathrm{s}})}{(k_{\mathrm{s}} + 2k_{\mathrm{f}}) + \psi(k_{\mathrm{f}} - k_{\mathrm{s}})}} 2\alpha^2 PrFG + \frac{Pr \cdot Ec}{Re \dfrac{(k_{\mathrm{s}} + 2k_{\mathrm{f}}) - 2\psi(k_{\mathrm{f}} - k_{\mathrm{s}})}{(k_{\mathrm{s}} + 2k_{\mathrm{f}}) + \psi(k_{\mathrm{f}} - k_{\mathrm{s}})} \cdot (1-\psi)^{2.5}} \cdot (4\alpha^2 F^2 + F'^2) = 0 \tag{13}$$

The Reynolds, Prandtl and Eckert numbers of the Jeffery-Hamel flow of nanofluids are introduced as

$$Re = \frac{u_{\mathrm{c}} \cdot \alpha}{v_{\mathrm{f}}},\ \begin{cases} u_{\mathrm{c}} > 0,\ \alpha > 0,\ \text{Divergent channel} \\ u_{\mathrm{c}} < 0,\ \alpha < 0,\ \text{Convergent channel} \end{cases} \tag{14}$$

$$Pr = \frac{\rho_{\mathrm{f}} \cdot (c_p)_{\mathrm{f}} \cdot u_{\mathrm{c}}}{K_{\mathrm{f}}} \tag{15}$$

$$Ec = \frac{\alpha \cdot u_{\mathrm{c}}^2}{(c_p)_{\mathrm{f}} \cdot T_{\mathrm{W}}} \tag{16}$$

The boundary conditions of the nanofluid flow and heat transfer between nonparallel plates in terms of $F(\eta)$ and $G(\eta)$ are expressed as follows:

At the centerline of channel:

$$F(0)=1,\ F'(0)=0,\ G'(0)=0 \tag{17}$$

At the body of channel:

$$F(1)=0,\ G(1)=1 \tag{18}$$

Based on the wall shear stress $\tau_w = \mu_{nf}\left(\frac{1}{r}\cdot\frac{\partial u}{\partial\theta}\right)\Big|_{\theta=\alpha}$, the skin friction coefficient C_f is defined as

$$C_f = \frac{\tau_W}{\rho\cdot u_c^2} \tag{19}$$

On the other hand, Nusselt number is expressed as follows:

$$Nu = \frac{r\cdot q_w\,|_{\theta=\alpha}}{K\cdot T_W} \tag{20}$$

where q_w is heat flux ($q_w = -K_{nf}\cdot\left(\frac{\partial T}{\partial r}+\frac{1}{r}\cdot\frac{\partial T}{\partial\theta}\right)$).

By using the dimensionless parameters Eq. (11), Eqs. (19) and (20) become

$$C_f = \frac{1}{Re(1-\psi)^{2.5}}\cdot F'(1) \tag{21}$$

$$Nu = \frac{K_{nf}}{K_f}\cdot[2-\frac{G'(1)}{\alpha}] \tag{22}$$

3 Basic idea of Adomian decomposition method

Consider the differential equation:

$$Lu + Ru + Nu = g(t) \tag{23}$$

where N is a nonlinear operator, L is the highest ordered derivative and R represents the remainder of linear operator L.

By considering L^{-1} as an n-fold integration for an nth order of L, the principles of method consists of applying the operator L^{-1} to the expression (23). Indeed, we obtain

$$L^{-1}Lu = L^{-1}g - L^{-1}Ru - L^{-1}Nu \tag{24}$$

The solution of Eq. (24) is given by

$$u = \varphi + L^{-1}g - L^{-1}Ru - L^{-1}Nu \tag{25}$$

where φ is determined from the boundary or initial conditions.

For the standard Adomian decomposition method, the solution u can be determined as the infinite series with the components given by

$$u = \sum_{n=0}^{\infty} u_n \tag{26}$$

And the nonlinear term Nu is given as follows:

$$Nu = \sum_{n=0}^{+\infty} A_n\ (u_0,\ u_1,\ \cdots,\ u_n) \tag{27}$$

where A_n, called Adomian polynomials, has been introduced by ADOMIAN [33] by the recursive formula:

$$A_n(u_0, u_1, \cdots, u_n) = \frac{1}{n!}\left[\frac{\mathrm{d}^n}{\mathrm{d}\lambda^n}\left[N\left(\sum_{n=0}^{\infty}\lambda^i\ u_i\right)\right]\right]_{\lambda=0},$$
$$n=0,\ 1,\ 2,\ \cdots \tag{28}$$

By substituting the given series Eqs. (28), (29) into both sides of Eq. (27), we obtain the following expressions:

$$\sum_{n=0}^{\infty}u_n = \varphi + L^{-1}g - L^{-1}R\sum_{n=0}^{\infty}u_n - L^{-1}\sum_{n=0}^{+\infty}A_n \tag{29}$$

According to Eq. (29), the recursive expression which defines the ADM components u_n is given as

$$u_0 = \varphi + L^{-1}g,\ u_{n+1} = -L^{-1}(Ru_n + A_n) \tag{30}$$

Finally, after some iterations, the solution of the studied equation can be given as an infinite series by

$$u=u_0+ u_1+ u_2+ u_3+\cdots+ u_n \tag{31}$$

The main advantage of this powerful analytical technique is to obtain the solution of nonlinear problems as a fast convergent series with elegantly computable terms and does not need linearization, discretization or restrictive assumptions.

4 Application of ADM to Jeffery-Hamel problem of nanofluid

In this section, we will apply the Adomian decomposition method to ordinary nonlinear differential equations (12) and (13) governing velocity and heat transfer of nanofluid flow between nonparallel plane walls. In fact, to solve the studied problem using ADM, we choose linear operators as the following expressions:

$$L_1 = \frac{\mathrm{d}^3}{\mathrm{d}\eta^3} \tag{32}$$

$$L_2 = \frac{\mathrm{d}^2}{\mathrm{d}\eta^2} \tag{33}$$

By considering Eqs. (32) and (33), Eqs. (12) and (13) could be expressed as

$$L_1F = -2Re\cdot\alpha\cdot\left[(1-\psi)^{2.5}\cdot(1-\psi+\psi\cdot\frac{\rho_s}{\rho_f})\right]\cdot$$
$$FF' + 4\alpha^2F' \tag{34}$$

$$L_2G + \frac{Pr\cdot Ec}{Re\cdot\frac{(k_s+2k_f)-2\psi(k_f-k_s)}{(k_s+2k_f)+\psi(k_f-k_s)}\cdot(1-\psi)^{2.5}}\cdot$$
$$(4\alpha^2F^2 + F'^2) = -4\alpha^2G - 2\alpha^2\cdot$$

$$\frac{(1-\psi)+\psi\cdot\dfrac{\rho_{\mathrm{s}}\cdot(c_p)_{\mathrm{s}}}{\rho_{\mathrm{f}}\cdot(c_p)_{\mathrm{f}}}}{\dfrac{(k_{\mathrm{s}}+2k_{\mathrm{f}})-2\psi(k_{\mathrm{f}}-k_{\mathrm{s}})}{(k_{\mathrm{s}}+2k_{\mathrm{f}})+\psi(k_{\mathrm{f}}-k_{\mathrm{s}})}}PrFG \tag{35}$$

The inverses of the operators L_1 and L_2 can be integrated from 0 to η and have the following form:

$$L_1^{-1}=\int_0^{\eta}\int_0^{\eta}\int_0^{\eta}(\cdot)\mathrm{d}\eta\mathrm{d}\eta\mathrm{d}\eta \tag{36}$$

$$L_2^{-1}=\int_0^{\eta}\int_0^{\eta}(\cdot)\mathrm{d}\eta\mathrm{d}\eta \tag{37}$$

Operating with L_1^{-1} and L_2^{-1} on Eqs. (34) and (35) and after exerting boundary conditions on them, we obtain:

$$F(\eta)=F(0)+F'(0)\eta+F''(0)\frac{\eta^2}{2}+L^{-1}(N_f) \tag{38}$$

$$G(\eta)=G(0)+L^{-1}(N_g) \tag{39}$$

where

$$N_f=2Re\cdot\alpha[(1-\psi)^{2.5}\cdot(1-\psi+\psi\frac{\rho_{\mathrm{s}}}{\rho_{\mathrm{f}}})]\cdot FF'+4\alpha^2F' \tag{40}$$

$$N_g=-4\alpha^2G-2\alpha^2\frac{(1-\psi)+\psi\dfrac{\rho_{\mathrm{s}}\cdot(c_p)_{\mathrm{s}}}{\rho_{\mathrm{f}}\cdot(c_p)_{\mathrm{f}}}}{\dfrac{(k_{\mathrm{s}}+2k_{\mathrm{f}})-2\psi(k_{\mathrm{f}}-k_{\mathrm{s}})}{(k_{\mathrm{s}}+2k_{\mathrm{f}})+\psi(k_{\mathrm{f}}-k_{\mathrm{s}})}}PrFG \tag{41}$$

On the other hand, by applying the boundary conditions, we have

$$F(\eta)=\sum_{n=0}^{\infty}F_n=F_0+L^{-1}(N_f) \tag{42}$$

$$G(\eta)=\sum_{n=0}^{\infty}G_n=G_0+L^{-1}(N_g) \tag{43}$$

where F_0 and G_0 have the following form:

$$F_0=1+a\frac{\eta^2}{2} \tag{44}$$

$$G_0=b+\frac{1}{2Re(1-\psi)^{2.5}\dfrac{(k_{\mathrm{s}}+2k_{\mathrm{f}})-2\psi(k_{\mathrm{f}}-k_{\mathrm{s}})}{(k_{\mathrm{s}}+2k_{\mathrm{f}})+\psi(k_{\mathrm{f}}-k_{\mathrm{s}})}}\cdot Ec\cdot Pr\cdot(F'^2+4\alpha^2F^2)\eta^2 \tag{45}$$

For the above problem, by applying the recursive formula (30) of ADM, the terms of Adomian polynomials are expressed as

$$A_0=-2a((1-\psi)+(\frac{\rho_{\mathrm{s}}}{\rho_{\mathrm{f}}})\psi)(1-\psi)^{2.5}Re\alpha\eta-4a\alpha^2\eta-a^2((1-\psi)+(\frac{\rho_{\mathrm{s}}}{\rho_{\mathrm{f}}})\psi)(1-\psi)^{2.5}Re\alpha\eta^3 \tag{46}$$

$$\begin{aligned}A_1=&\frac{2}{3}a(((1-\psi)+(\frac{\rho_{\mathrm{s}}}{\rho_{\mathrm{f}}})\psi)(1-\psi)^{2.5})^2Re\alpha^2\eta^3+\\&\frac{8}{3}a((1-\psi)+(\frac{\rho_{\mathrm{s}}}{\rho_{\mathrm{f}}})\psi)(1-\psi)^{2.5}Re\alpha^3\eta^3+\frac{8}{3}a\alpha^4\eta^3+\\&\frac{3}{5}a^2(((1-\psi)+(\frac{\rho_{\mathrm{s}}}{\rho_{\mathrm{f}}})\psi)(1-\psi)^{2.5})^2Re^2\alpha^2\eta^5+\\&\frac{6}{5}a^2((1-\psi)+(\frac{\rho_{\mathrm{s}}}{\rho_{\mathrm{f}}})\psi)(1-\psi)^{2.5})Re\alpha^3\eta^7+\\&\frac{1}{15}a^3(((1-\psi)+(\frac{\rho_{\mathrm{s}}}{\rho_{\mathrm{f}}})\psi)(1-\psi)^{2.5})^2Re^2\alpha^2\eta^5\end{aligned} \tag{47}$$

$$B_0=(-4\alpha^2-\frac{2}{\mathrm{A}}(FBPr\alpha^2))(b-\frac{1}{2Re(1-\psi)^{2.5}A}\cdot(Ec\cdot Pr\cdot(F'^2+4\alpha^2F^2)\eta^2)) \tag{48}$$

$$\begin{aligned}B_1=&-\frac{1}{Re(1-\psi)^{2.5}A^3}(2A+FBPr)\alpha^2\eta^2\{F'^2\cdot Ec\cdot Pr\cdot\\&[0.166667FBPr\alpha^2\eta^2+A(-1+0.333333\alpha^2\eta^2)]+\\&\alpha^2[b(1-\psi)^{2.5}A(-4A-2FBPr)Re+EcF^2Pr(-4A+\\&1.33333A\alpha^2\eta^2+0.666667FBPr\alpha^2\eta^2)]\}\end{aligned} \tag{49}$$

Therefore, the first iterations of solutions are expressed as follows:

$$F_0=1+\frac{a\eta^2}{2} \tag{50}$$

$$G_0=b+\frac{1}{2Re(1-\psi)^{2.5}\dfrac{(k_{\mathrm{s}}+2k_{\mathrm{f}})-2\psi(k_{\mathrm{f}}-k_{\mathrm{s}})}{(k_{\mathrm{s}}+2k_{\mathrm{f}})+\psi(k_{\mathrm{f}}-k_{\mathrm{s}})}}\cdot Ec\cdot Pr\cdot(F'^2+4\alpha^2F^2)\eta^2 \tag{51}$$

$$\begin{aligned}F_1=&-\frac{1}{12}a((1-\psi)+(\frac{\rho_{\mathrm{s}}}{\rho_{\mathrm{f}}})\psi)(1-\psi)^{2.5}Re\alpha\eta^4-\\&\frac{1}{6}a\alpha^2\eta^4-\frac{1}{120}a^2((1-\psi)+(\frac{\rho_{\mathrm{s}}}{\rho_{\mathrm{f}}})\psi)(1-\psi)^{2.5}Re\alpha\eta^6\end{aligned} \tag{52}$$

$$\begin{aligned}G_1=&-(\frac{1}{2Re(1-\psi)^{2.5}A})F'^2\cdot Ec\cdot Pr\cdot\eta^2-2b\alpha^2\eta^2-\\&\frac{1}{A}bFBPr\alpha^2\eta^2-\frac{2}{Re(1-\psi)^{2.5}A}EcF^2\,2Pr\alpha^2\eta^2+\\&\frac{0.166667}{Re(1-\psi)^{2.5}A}F'^2\cdot Ec\cdot Pr\cdot\alpha^4\eta^4+\\&\frac{0.0833333}{Re(1-\psi)^{2.5}A^2}F'^2\cdot Ec\cdot FB2Pr\alpha^2\eta^4+\\&\frac{0.666667}{Re(1-\psi)^{2.5}A}Ec\cdot F^2Pr\cdot\alpha^4\eta^4+\\&\frac{0.333333}{Re(1-\psi)^{2.5}A^2}Ec\cdot F^3BPr^2\alpha^4\eta^4\end{aligned} \tag{53}$$

with

$$A=\frac{(k_s+2k_f)-2\psi(k_f-k_s)}{(k_s+2k_f)+\psi(k_f-k_s)} \tag{54}$$

$$B=(1-\psi)+\psi\cdot\frac{\rho_s(c_p)_s}{\rho_f(c_p)_f} \tag{55}$$

Finally, the approximate solution for nanofluid flow and heat transfer in Jeffery-Hamel problem could be expressed as

$$F(\eta)=F_0+F_1+F_2+F_3+\cdots+F_n \tag{56}$$

$$G(\eta)=G_0+G_1+G_2+G_3+\cdots+G_n \tag{57}$$

According to Eqs. (56) and (57), it is worth noting that the accuracy of ADM solutions increases by increasing the number of iterations term (n). On the other hand, the constants a and b could be determined with boundary conditions Eqs. (17) and (18).

5 Results and discussion

In this work, nanofluid flow and heat transfer between inclined walls are studied analytically. An efficient technique of computation, namely the Adomian decomposition method, is employed to solve the governing equations. The thermophysical properties of Cu-water nanofluid are given in Table 1.

Table 1 Thermophysical properties of Cu-water nanofluid

Material	ρ/(kg·m^{-3})	c_p/(J·kg^{-1}·K^{-1})	K/(W·m^{-1}·K^{-1})
Water	997.1	4179	0.613
Cu	8933	385	401

Effect of Reynolds number, Re, on the velocity profile for convergent flow is depicted in Fig. 2. Indeed, increasing Reynolds number leads, on one hand, to a flatter profile at the centre of channel with high gradients near the walls, and on the other hand, to decreased thickness of the momentum boundary layer. We notice also that the velocity profiles are symmetric against η=0 and the symmetric convergent flow is possible for an opening angle, 2α, not exceeding π. It is also clear for convergent channel that the backflow is entirely excluded. On the other hand, the effect of Reynolds number on divergent flow (Fig. 3) is to concentrate the volume flux at the centre of channel with smaller gradients near the walls and consequently the thickness of momentum boundary layer increases. For purely divergent channel, the symmetric flow is not possible for an opening angle, 2α, unless Reynolds number does not exceed a critical value. Above this critical value, the separation and backflow phenomena are started.

Figures 4–5 show the effect of channel half-angle, α, on the velocity profiles in convergent and divergent channels. It is found that the behaviour of velocity is predicted to be similar to that observed in Figs. 2–3. Indeed, in converging channel (Fig. 4), we can see that the increase of α leads to an increase of favourable pressure gradient, while in diverging channel (Fig. 5), we can clearly observe that, with increasing of α, the backflow phenomenon is started when the adverse pressure gradient is large enough.

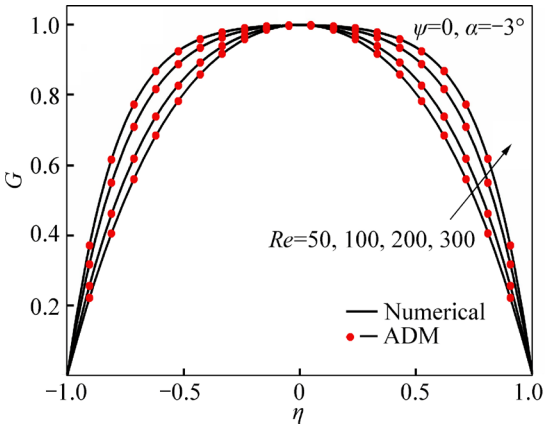

Fig. 2 Effect of Reynolds number, Re, on velocity profile in converging channel

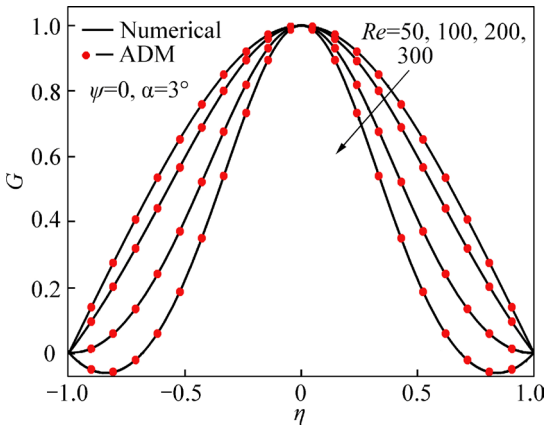

Fig. 3 Effect of Reynolds number, Re, on velocity profile in diverging channel

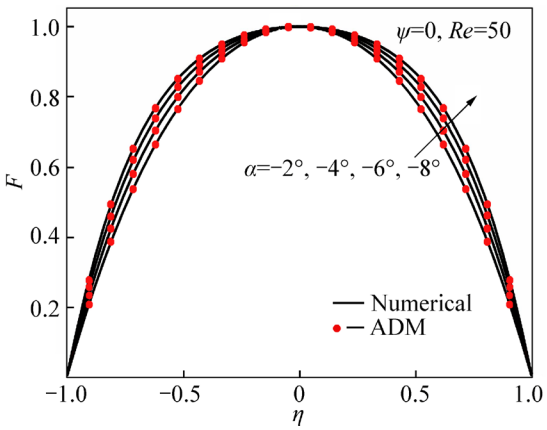

Fig. 4 Effect of channel half-angle, α, on velocity profile in converging channel

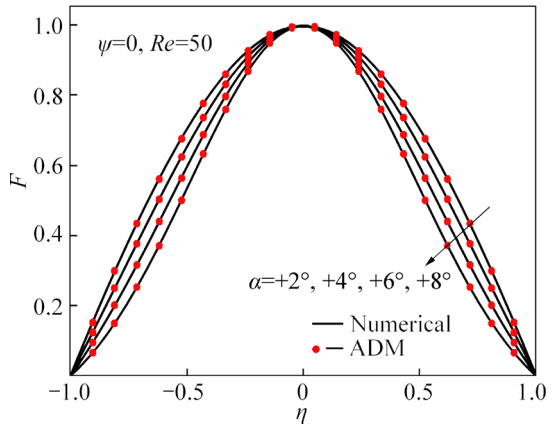

Fig. 5 Effect of channel half-angle, α, on velocity profile in diverging channel

Effect of copper nanoparticles on the velocity profiles for a convergent-divergent channel (when Re=200 and α=±3°) is displayed in Figs. 6 and 7, respectively. In fact, Fig. 6 reveals that the velocity in convergent channel increases when nanoparticle volume fraction increases; however, in the case of divergent channel (Fig. 7), it appears that the velocity is a decreasing function of nanoparticle volume fraction. It

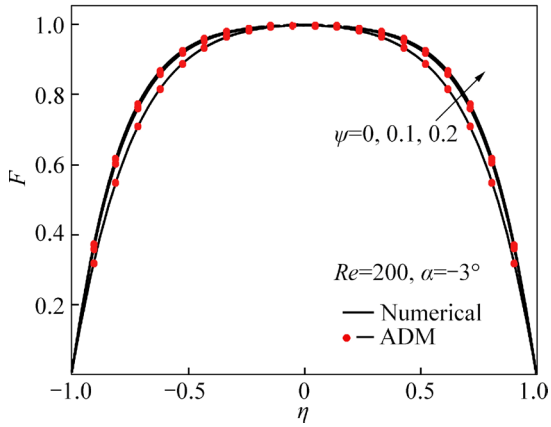

Fig. 6 Effect of nanoparticle volume fraction, ψ, on velocity profile in converging channel

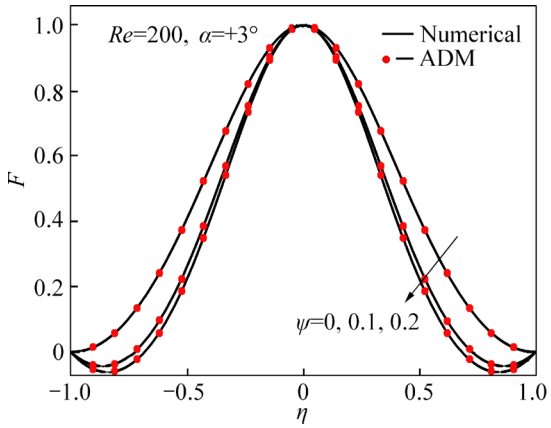

Fig. 7 Effect of nanoparticle volume fraction, ψ, on velocity profile in diverging channel

can be clearly seen that the backflow phenomenon may occur for high values of Reynolds number when the volume fraction of the nanoparticle increases.

Effects of Reynolds number, Re, nanoparticle volume fraction, ψ, the channel half-angle, α, and Eckert number, Ec, on the evolution of skin friction, Nusselt number and the temperature profiles are displayed in Figs. 8–20.

Effects of Reynolds number and the channel half-angle (when Pr=7, Ec=0.6 and ψ=0.1) for a

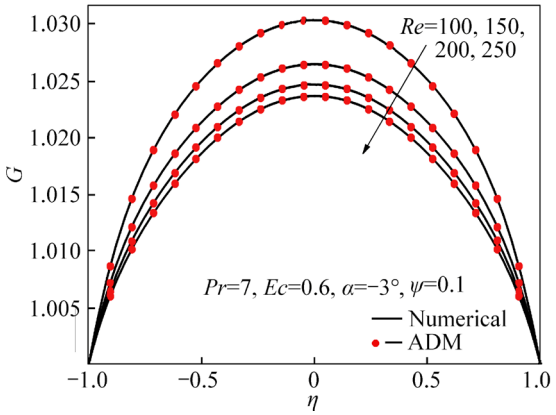

Fig. 8 Effect of Reynolds number, Re, on temperature distribution in converging channel

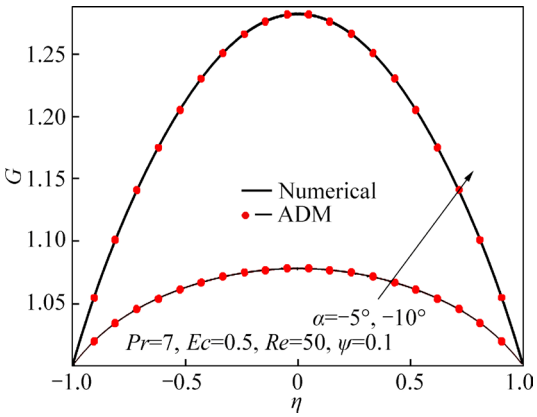

Fig. 9 Effect of channel half-angle, α, on temperature distribution in converging channel

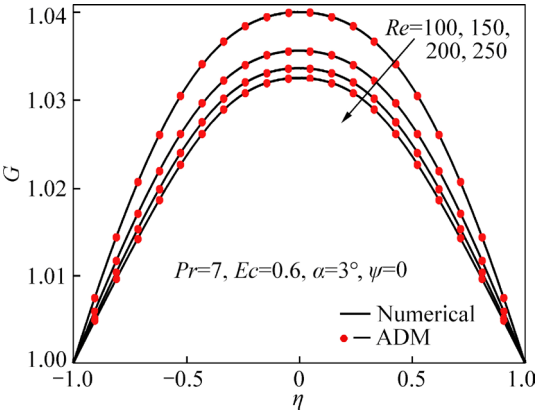

Fig. 10 Effect of Reynolds number, Re, on temperature distribution in diverging channel

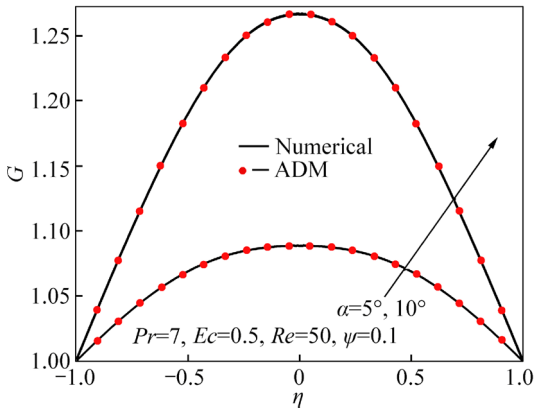

Fig. 11 Effect of channel half-angle, α, on temperature distribution in diverging channel

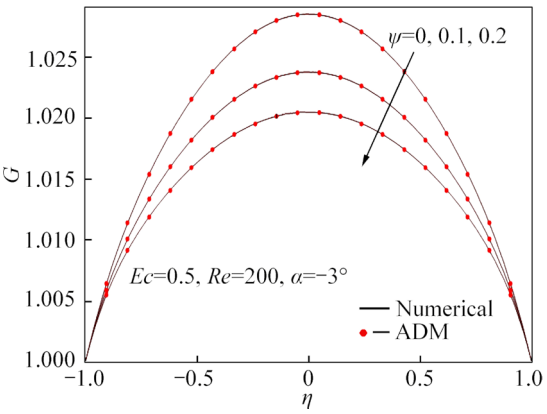

Fig. 12 Effect of nanoparticle volume fraction, ψ, on temperature distribution in converging channel

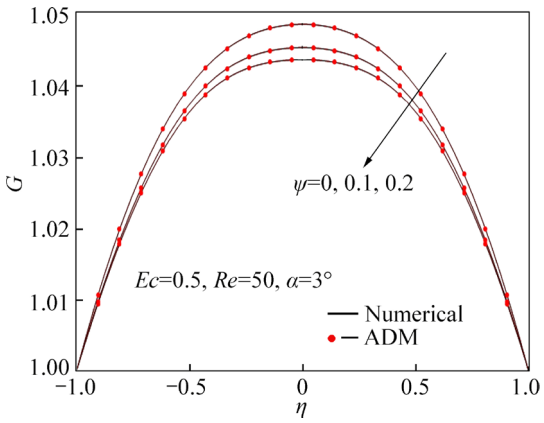

Fig. 13 Effect of nanoparticle volume fraction, ψ, on temperature distribution in diverging channel

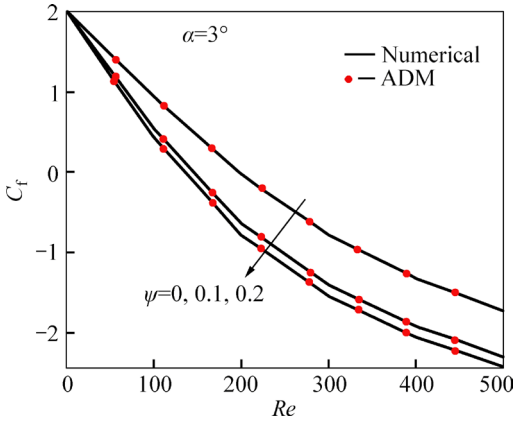

Fig. 14 Effects of Reynolds number, Re, and nanoparticle volume fraction, ψ, on skin friction coefficient

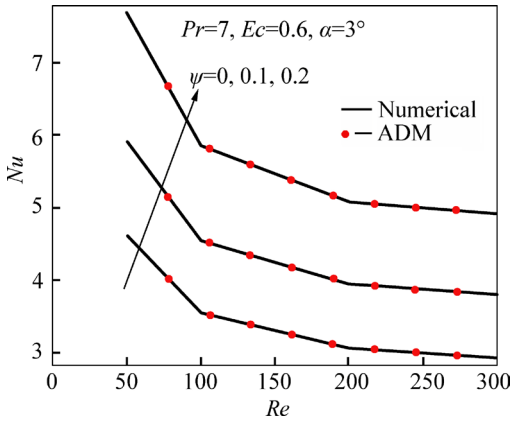

Fig. 15 Effects of Reynolds number, Re, and nanoparticle volume fraction, ψ, on Nusselt number

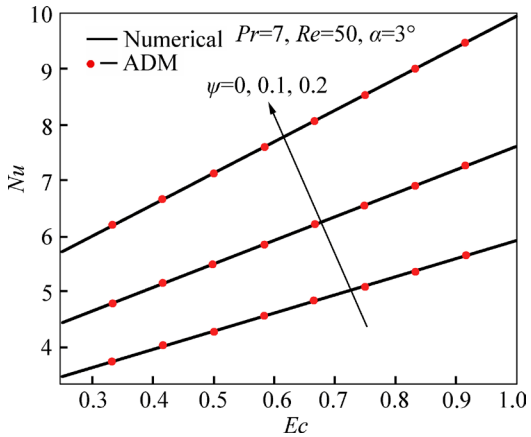

Fig. 16 Effects of Eckert number, Ec, and nanoparticle volume fraction, ψ, on Nusselt number

convergent and divergent channel, are depicted in Figs. 8–11. It can be seen for convergent channel (Figs. 8 and 9) that the thermal boundary layer thickness is decreased as the magnitude of Reynolds number Re increases; while the thermal boundary layer thickness is an increasing function of the channel half-angle, α. On the other hand, as depicted in Figs. 10 and 11 for the case of a divergent channel (when α=3°, Pr=7 and Ec=0.6), it is well seen that increase of both of the Reynolds number and the channel half-angle makes an increase in the thickness of thermal boundary layer.

Effect of nanoparticle volume fraction on temperature profiles is depicted in Figs. 12 and 13. It is well known that the presence of nanoparticles leads to increased thermal conductivity of the nanofluids. This increase is mainly accompanied by an increase in thermal diffusivity and consequently a drop in temperature gradients occurs, which leads to increase in

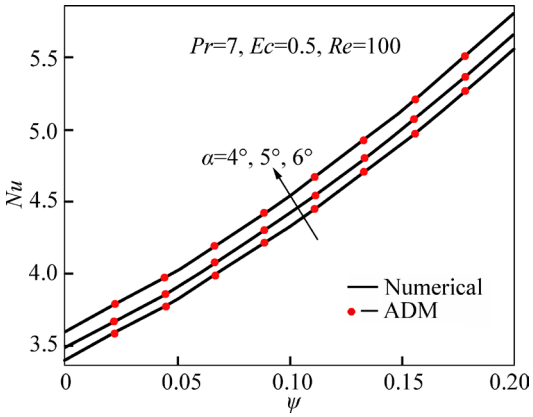

Fig. 17 Effects of channel half-angle, α, and nanoparticle volume fraction, ψ, on Nusselt number

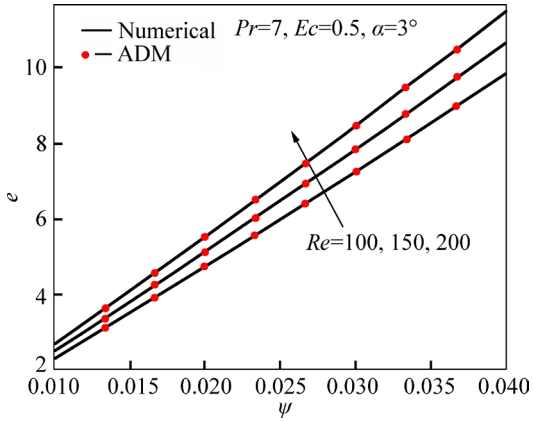

Fig. 18 Effects of Reynolds number, Re, and nanoparticle volume fraction, ψ, on enhancement heat transfer

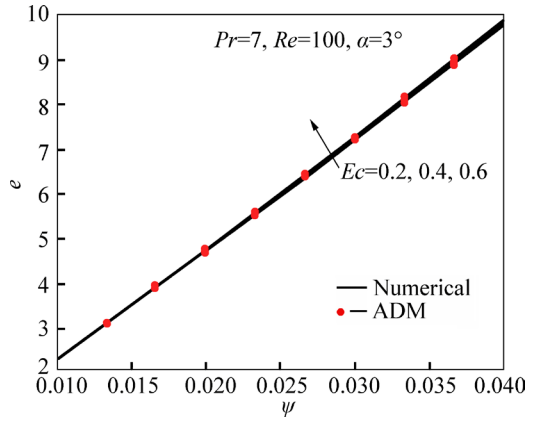

Fig. 19 Effects of Eckert number, Ec, and nanoparticle volume fraction, ψ, on enhancement heat transfer

the thickness of thermal boundary layer for both convergent and divergent channels.

Effects of Reynolds number, Re, and volume fraction of nanofluid, ψ, on skin friction coefficient are drawn in Fig. 14. In fact, results show that the magnitude of skin friction decreases with the increase of both of the Reynolds number and the nanofluid volume fraction. On the other hand, it can be clearly seen that the backflow starts with apparition of negative values of skin friction

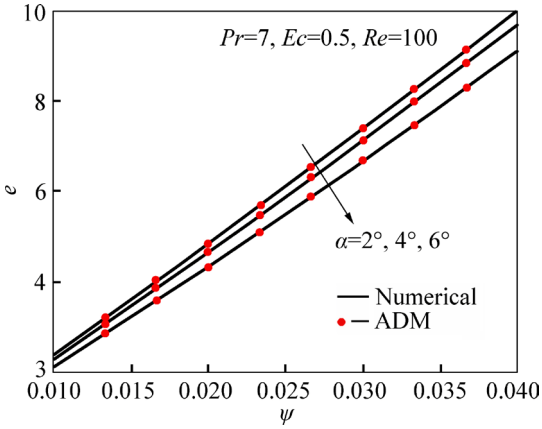

Fig. 20 Effects of channel half-angle, α, and nanoparticle volume fraction, ψ, on enhancement heat transfer

coefficient.

Figure 15 displays the effect of Reynolds number on Nusselt number. As shown above (Fig. 10), increased Reynolds number leads to the increase of thermal boundary layer thickness; therefore, Nusselt number appears as a decreasing function of Reynolds number, Re. The behaviour of Nusselt number, Nu, versus Eckert number, Ec, is quite different. Indeed, as shown in Fig. 16, we notice an increase in magnitude of Nusselt number with increase of Eckert number. This can be explained by the presence of viscous dissipation, which leads to an increase in magnitude of temperature, and, consequently the increase in Nusselt number is observed. Figure 17 depicts the effect of channel half-angle on Nusselt number. It can be seen that increasing the channel half-angle causes an increase in thermal boundary layer thickness (see Fig. 11) and consequently leads to an increase in Nusselt number.

It is also well known that Nusselt number is the ratio of convective to conductive heat transfer. On the other hand, convection includes both advection and diffusion. As mentioned above, a higher diffusivity leads to an increase in the thickness of thermal boundary layer. This increase can considerably reduce Nusselt number, however, as given in Eq. (22), Nusselt number is defined as a multiplication of thermal conductivity ratio (K_{nf}/K_f) and the temperature gradient. According to Figs. 15–17, an increase in Nusselt number is observed by increasing volume fraction of copper nanoparticles. In fact, with the presence of copper nanoparticles in a water base fluid, thermal conductivity ratio is bigger than reduction in temperature gradient and consequently an enhancement in Nusselt number is produced with increase of nanoparticle volume fraction.

Heat transfer enhancement due to the presence of copper nanoparticles is evaluated and results are reported in Figs. 18–20. In fact, this enhancement is calculated as follows:

$$e=\frac{Nu_{(\text{nanofluid})}-Nu_{(\text{base fluid})}}{Nu_{(\text{base fluid})}}\times 100$$

The enhancement evolution versus nanoparticle volume fraction, ψ, for different values of Reynolds number, Re, and Eckert number, Ec, is displayed in Figs. 18 and 19. Indeed, it is noticed that the enhancement increases with the increase of Reynolds number and Eckert number; however, it decreases with increase of the channel half-angle, α, as shown in Fig. 20.

In comparison of ADM solution with numerical results, it is found that results are similar to each other, which justifies and confirms validity, applicability and the higher accuracy of Adomian decomposition method. Tables 2–5 show numerical data of velocity and temperature distributions for a convergent and divergent channel when Re=50, α=±3°, Pr=7, Ec=0.6 and ψ=0.03. On the other hand, Tables 6–9 also give numerical data of velocity and temperature distributions when Re=100, α=±5°, Pr=7, Ec=0.6 and ψ=0.01. In these tables, the errors are introduced as follows:

$$E_1=\left|F(\eta)_{\text{Num}}-F(\eta)_{\text{ADM}}\right|$$

$$E_2=\left|G(\eta)_{\text{Num}}-G(\eta)_{\text{ADM}}\right|$$

Finally, according to the obtained results depicted in Tables 2–9, an excellent agreement between numerical Runge-Kutta method and Adomian decomposition method is clearly observed.

Table 2 Comparison between numerical and analytical results for velocity distribution in converging channel (Re=50, α=–3° and ψ=3%)

η	Numerical	ADM	E_1
–1	0.00000000000	0.00000000000	0.00000000000
–0.75	0.9568619246104294	0.9568615908529563	$3.337574731032688\times10^{-7}$
–0.5	0.8114573769442529	0.8114559074862294	0.000001469458023484193
–0.25	0.5158279952776336	0.5158243637441324	0.000036315335011360 97
0	1.00000000000	1.00000000000	0.00000000000
0.25	0.5158279952776336	0.5158243637441324	0.000036315335011360 97
0.5	0.8114573769442529	0.8114559074862294	0.000001469458023484193
0.75	0.9568619246104294	0.9568615908529563	$3.337574731032688\times10^{-7}$
1	0.00000000000	0.00000000000	0.00000000000

Table 3 Comparison between numerical and analytical results for velocity distribution in diverging channel (Re=50, α=3° and ψ=3%)

η	Numerical	ADM	E_1
–1	0.00000000000	0.00000000000	0.00000000000
–0.75	0.34617891945024026	0.34619249466793467	0.000013575217694440595
–0.5	0.6693201741166637	0.669327237913685	0.000070637970213116 57
–0.25	0.9097653427408956	0.9097672581403088	0.000019153994131881 9
0	1.00000000000	1.00000000000	0.00000000000
0.25	0.9097653427408956	0.9097672581403088	0.000019153994131881 9
0.5	0.6693201741166637	0.669327237913685	0.000070637970213116 57
0.75	0.34617891627424824	0.34619249466793467	0.000013578393686430879
1	0.00000000000	0.00000000000	0.00000000000

Table 4 Comparison between numerical and analytical results for thermal distribution in converging channel (Re=50, α=–3° and ψ=3%)

η	Numerical	ADM	E_2
–1	1.00000000000	1.00000000000	0.00000000000
–0.75	1.0226755380341845	1.02267456214785	$9.75886334630971\times10^{-7}$
–0.5	1.0311432179608124	1.031142143045987	0.000001074914825371919
–0.25	1.034488616758601	1.034487498214572	0.00000111854402895517
0	1.0354237076304937	1.035424987231457	0.000001279600963188798
0.25	1.034488616758601	1.034487498214572	0.00000111854402895517
0.5	1.0311432179608124	1.031142143045987	0.000001074914825371919
0.75	1.0226755380341845	1.02267456214785	$9.75886334630971\times10^{-7}$
1	1.00000000000	1.00000000000	0.00000000000

Table 5 Comparison between numerical and analytical results for thermal distribution in diverging channel (Re=50, α=3° and ψ=3%)

η	Numerical	ADM	E_2
–1	1.00000000000	1.00000000000	0.00000000000
–0.75	1.0227929743872683	1.0227918020580276	0.000001172329240795022
–0.5	1.036453755744072	1.0364514226254804	0.00000233118591657523
–0.25	1.0420667601778564	1.0420640611590504	0.00002699018806007203
0	1.0432060494431412	1.0432033195693209	0.00002729873820328521
0.25	1.0420667601778564	1.0420640611590504	0.00002699018806007203
0.5	1.036453755744072	1.0364514226254804	0.00000233118591657523
0.75	1.0227929743872683	1.0227918020580276	0.000001172329240795022
1	1.00000000000	1.00000000000	0.00000000000

Table 6 Comparison between numerical and analytical results for velocity distribution in converging channel (Re=100, α=–5° and ψ=1%)

η	Numerical	ADM	E_1
–1	0.00000000000	0.00000000000	0.00000000000
–0.75	0.680935867130178	0.680935597321428	$2.69808749897570\times10^{-7}$
–0.5	0.9153966003670116	0.9153963132569125	$2.871101016932442\times10^{-7}$
–0.25	0.9851250287096571	0.9851254012398745	$3.725302173407385\times10^{-7}$
0	1.00000000000	1.00000000000	0.00000000000
0.25	0.9851250287096571	0.9851254012398745	$3.725302173407385\times10^{-7}$
0.5	0.9153966003670116	0.9153963132569125	$2.871101016932442\times10^{-7}$
0.75	0.680935867130178	0.680935597321428	$2.69808749897570\times10^{-7}$
1	0.00000000000	0.00000000000	0.00000000000

Table 7 Comparison between numerical and analytical results for velocity distribution in diverging channel (Re=100, α=5° and ψ=1%)

η	Numerical	ADM	E_1
–1	0.00000000000	0.00000000000	0.00000000000
–0.75	0.05086374496916339	0.0508629832146875	$7.617544758933836\times10^{-7}$
–0.5	0.3449786943001594	0.3449774518351627	0.000001242464996720205
–0.25	0.7740537080551285	0.7740548514236578	0.000011143368529299415
0	1.000000000	1.000000000	0.000000000
0.25	0.7740537080551285	0.7740548514236578	0.000011143368529299415
0.5	0.3449786943001594	0.3449774518351627	0.000001242464996720205
0.75	0.05086374496916339	0.0508629832146875	$7.617544758933836\times10^{-7}$
1	0.00000000000	0.00000000000	0.00000000000

Table 8 Comparison between numerical and analytical results for thermal distribution in converging channel (Re=100, α=–5° and ψ=1%)

η	Numerical	ADM	E_2
–1	1.0000000000	1.0000000000	0.0000000000
–0.75	1.031104207748306	1.03110313698745	0.000001070760855981234
–0.5	1.0495480712958662	1.0495452314569875	0.000002839838878720968
–0.25	1.0604751591699018	1.0604726987453212	0.000002460424580519316
0	1.0641353188531641	1.0641333456789213	0.000001973174242886344
0.25	1.0604751591699018	1.0604726987453212	0.000002460424580519316
0.5	1.0495480712958662	1.0495452314569875	0.000002839838878720968
0.75	1.031104207748306	1.03110313698745	0.000001070760855981234
1	1.0000000000	1.0000000000	0.0000000000

Table 9 Comparison between numerical and analytical results for thermal distribution in diverging channel (Re=100, α=5° and ψ=1%)

η	Numerical	ADM	E_2
–1	1.0000000000	1.0000000000	0.0000000000
–0.75	1.0276466580371744	1.027643265417895	0.0000033926192792854
–0.5	1.0515856680371445	1.051588213654789	0.0000025456654444422
–0.25	1.0665953697611374	1.0665936987436522	0.0000016710174852718
0	1.0707850923679623	1.0707843215864798	$7.70781482417604\times10^{-7}$
0.25	1.0665953697611374	1.0665936987436522	0.0000016710174852718
0.5	1.0515856680371445	1.051588213654789	0.0000025456654444422
0.75	1.0276466580371744	1.027643265417895	0.0000033926192792854
1	1.0000000000	1.0000000000	0.0000000000

6 Conclusions

1) Increasing Reynolds number of a convergent flow leads to a flatter profile at the centerline of channel and consequently the thickness of momentum boundary layer decreases with the increase of Reynolds number.

2) Effect of increasing Reynolds number of a divergent flow is to concentrate the volume flux at the centerline of channel. Consequently, the thickness of momentum boundary layer increases with the increase of Reynolds number.

3) The behaviour of velocity under the effect of varying channel half-angle, α, is predicted to be similar to that observed in the case of varying Reynolds number for both convergent and divergent flows.

4) The backflow phenomenon is entirely excluded in a convergent channel; however, this phenomenon may occur at high values of the channel half-angle, α, and Reynolds number, Re, in a diverging channel.

5) Skin friction coefficient decreases with the increase of both of the Reynolds number and the nanoparticles volume fraction.

6) The magnitude of Nusselt number increases with the increase of Eckert number and the channel half-angle; however, it decreases with the increase of Reynolds number.

7) The presence of copper nanoparticles in a water base fluid enhances significantly the heat transfer characteristics. Consequently, the Nusselt number increases as nanoparticle volume fraction increases.

8) An excellent agreement between Adomian decomposition method and numerical Runge-Kutta method is observed, thus justifying validity, applicability and higher accuracy of the used analytical method.

References

[1] JEFFERY G B. The two dimensional steady motion of a viscous fluid [J]. Phil Mag, 1915, 29: 455–465.

[2] HAMEL G. Spiralformige bewegungen zaher flussigkeiten [J]. Jahresbericht der deutshen Math Vereiniguug, 1916, 25: 34–60. (in German)

[3] ROSENHEAD L. The steady two-dimensional radial flow of viscous fluid between two inclined plane walls [J]. Proc R Soc London, 1940, A175: 436–467.

[4] MILLSAPS K, POHLHAUSEN K. Thermal distributions in Jeffery-Hamel flows between non-parallel plane walls [J]. J Aero Sci, 1953, 20: 187–196.

[5] FRAENKEL L E. Laminar flow in symmetrical channels with slightly curved walls. I. On the Jeffery-Hamel solutions for flow between plane walls [J]. Proc R Soc London, 1963, A267: 119–138.

[6] SHEIKHOLESLAMI M, GANJI D D, ASHORYNEJAD H R, ROKNI H B. Analytical investigation of Jeffery-Hamel flow with high magnetic field and nanoparticle by Adomian decomposition method [J]. Appl Math Mech–Engl Ed, 2012, 33(1): 1553–1564.

[7] HATAMI M, SHEIKHOLESLAMI M, HOSSEINI M, GANJI D D. Analytical investigation of MHD nanofluid flow in non-parallel walls [J]. Journal of Molecular Liquids, 2014, 194: 251–259.

[8] ELLAHI R, MUBASHIR BHATTI M, RIAZ A, SHEIKHOLESLAMI M. Effects of magnetohydrodynamics on peristaltic flow of Jeffrey fluid in a rectangular duct through a porous medium [J]. Journal of Porous Media, 2014, 17(2): 143–157.

[9] BATCHELOR G K. An introduction to fluid dynamics [M]. Cambridge University Press, 1967.

[10] WHITE F M. Viscous fluid flow [M]. Mc Graw Hill, 1974.

[11] H. SSHLICHTING H, GERSTEN K. Boundary layer theory [M]. 8th revised edition. Springer, 2000.

[12] CHOI S U S. Enhancing thermal conductivity of fluids with nanoparticles in developments and application of non Newtonian flows [J]. ASME FED-vol. 231/MD, 1995, 66: 99–105.

[13] MURSHED S M S, LEONG K C, YANG C. Enhanced thermal conductivity of TiO_2-water based nanofluids [J]. International Journal of Thermal Sciences, 2005, 44: 367–373.

[14] HONG T, YANG H, CHOI C J. Study of the enhanced thermal conductivity of Fe nanofluids [J]. Journal of Applied Physics, 2005: 064311-1–064311-4.

[15] XIE H, ANG J, XI T, LIU Y, AI F, WU Q. Thermal conductivity enhancement of suspensions containing nanosized alumina particles [J]. Journal of Applied Physics, 2002, 91: 4568–4572.

[16] WANG Y, AVIDSON J L, JIANG L. Thermal conductivity of nanoparticle suspensions [C]// Proceedings of 8th AIAA/ASME Joint Thermophysics and Heat Transfer Conference USA, 2002: 10. 2514/6. 2002−3345.

[17] PAK B C, CHO Y I. Hydrodynamic and heat transfer study of dispersed fluids with submicron metallic oxide particles [J]. Exp Heat Transfer, 1998, 11: 151–170.

[18] XUAN Y, LI Q. Investigation on convective heat transfer and flow features of nanofluids [J]. J Heat transfer, 2003, 125: 151–155.

[19] HE Y, JIN Y, CHEN H, DING Y, CANG D, LU H. Heat transfer and flow behaviour of aqueous suspensions of TiO_2 nanoparticles (nanofluids) flowing upward through a vertical pipe [J]. Int J Heat Mass Transfer, 2007, 50: 2272–2281.

[20] TORII S, YANG W J. Heat transfer augmentation of aqueous suspensions of nanodiamonds in turbulent pipe flow [J]. J Heat Transfer, 2009, 131: 043203-1−043203-5.

[21] SHEIKHOLESLAMI M, GANJI D D. Heat transfer of Cu-water nanofluid between parallel plates [J]. Powder Technology, 2013, 235: 873–879.

[22] KHANAFER K, VAFAI K, LIGHTSTONE M. Buoyancy-driven heat transfer enhancement in a two-dimensional enclosure utilizing nanofluids [J]. International Journal of Heat and Mass Transfer, 2003, 46: 3639–3653.

[23] KUZNETSOV A V, NIELD D. Natural convection boundary layer flow of nanofluid past a vertical plate [J]. Int J Thermal Sci, 2010, 49: 243–247.

[24] SHEIKHOLESLAMI M. KKL correlation for simulation of nanofluid flow and heat transfer in a permeable channel [J]. Physics Letters, 2014, A 378: 3331–3339.

[25] SHEIKHOLESLAMI M. Effect of spatially variable magnetic field on ferrofluid flow and heat transfer considering constant heat flux boundary condition [J]. European Physical Journal Plus, 2014, 11: 129–248.

[26] SHEIKHOLESLAMI M, GANJI D D. Nanofluid flow and heat transfer between parallel plates considering Brownian motion using DTM. Comput [J]. Methods Appl Mech Engrg, 2015, 283: 651–663.

[27] SHEIKHOLESLAMI M, GANJI D D. Entropy generation of nanofluid in presence of magnetic field using Lattice Boltzmann Method [J]. Physica A, 2015, 417: 273–286.

[28] SHEIKHOLESLAMI M, GANJI D D. Ferrohydrodynamic and Magnetohydrodynamic effects on ferrofluid flow and convective heat transfer [J]. Energy, 2014, 75: 400–410.

[29] LIAO S J. Beyond perturbation: Introduction to homotopy analysis method [M]. Boca Raton: Chapman and Hall/CRC Press, 2003.

[30] HE J H. Homotopy perturbation method: A new nonlinear analytical technique [J]. Appl Math Comput, 2003, 135: 73–79.

[31] HE J H, WU X H. Variational iteration method: New development and applications [J]. Computers and Mathematics with Applications, 2007, 54: 881–894.

[32] HE J H. Variational iteration method-Some recent results and new interpretations [J]. Journal of Computational and Applied Mathematics, 2007, 207: 3–17.

[33] ADOMIAN G. Solving frontier problems of physics: The decomposition method [M]. Kluwer Academic Publishers, Dodrecht, 1994.

[34] RASHIDI M M, DINARVAND S. Purely analytic approximate solutions for steady three-dimensional problem of condensation film on inclined rotating disk by homotopy analysis method [J]. Nonlinear Analysis: Real world applications, 2009, 10: 2346–2356.

[35] BEONG I N, YUN B I. Intuitive approach to the approximate analytical solution for the Blasius problem [J]. Applied Mathematics and Computation, 2010, 215: 3489–3494.

[36] WAZWAZ A M. The variational iteration method for solving two forms of Blasius equation on a half-infinite domain [J]. Applied Mathematics and Computation, 2007, 188: 485–491.

[37] DOMAIRRY G, MOHSENZADEH A, FAMOURI M. The application of homotopy analysis method to solve nonlinear differential equation governing Jeffery-Hamel flow [J]. Communications in Nonlinear Science and Numerical Simulation, 2009, 14: 85–95.

[38] JONEIDI A A, DOMAIRRY G, BABAELAHI M. Three analytical methods applied to Jeffery-Hamel flow [J]. Communications in Nonlinear Science and Numerical Simulation, 2010, 15: 3423–3434.

[39] ESMAILI Q, RAMIAR A, ALIZADEH E, GANJI D D. An approximation of the analytical solution of the Jeffery–Hamel flow by decomposition method [J]. Physics Letters, 2008, A372: 3434–3439.

[40] GANJI Z Z, GANJI D D, ESMAEILPOUR M. Study on nonlinear Jeffery–Hamel flow by He's semi-analytical methods and comparison with numerical results [J]. Computers and Mathematics with Applications, 2009, 58: 2107–2116.

(Edited by YANG Bing)